JMEPEG (2018) 27:6349–6364
https://doi.org/10.1007/s11665-018-3683-1

1059-9495/$19.00

The Effects of Alloying Elements on the Continuous Cooling Transformation Behavior of 2¼Cr-1Mo Steels

John M. Tartaglia, Alison N. Kuelz, and Veronica Hatty Thelander

(Submitted June 1, 2018; in revised form July 30, 2018; published online October 17, 2018)

The continuous cooling transformation (CCT) behavior of eight 2¼Cr-1Mo steels from a statistically designed matrix was determined. These steels contained two levels of carbon (0.07 and 0.16 wt.%), manganese (0.35 and 0.85%), chromium (1.5 and 2.8%), and molybdenum (0.3 and 1.25%). Each steel was tested in a quenching dilatometer at five to six cooling rates between 725 and 1.2 °C/min. For each CCT sample, the change in length, microstructure, and macrohardness were determined. The ferrite content was also measured for samples cooled near the ferrite nose. Pearson correlation and multiple regression analyses were performed for various CCT diagram parameters. The correlation analysis showed that carbon and chromium contents significantly affected the critical temperatures and the bainite and martensite transformation temperatures. Increasing carbon content significantly increased the hardness for the bainite and martensite range of cooling rates, but hardness at slower cooling rates was unaffected by alloying elements. Regression equations were obtained for the critical temperatures and the ferrite nose cooling rate.

Keywords 2¼Cr-1Mo steel, continuous cooling transformation behavior, effect of alloying elements, low-alloy steel

1. Introduction

Chromium–molybdenum steels are ubiquitous in the energy industry. In particular, Cr-Mo steel is used in fossil-fired power-generating plants, aircraft power plants, chemical processing plants, and petroleum-processing plants. These steels have ferrite–pearlite or ferrite–bainite microstructures and are used at temperatures up to 540 °C (1000 °F). Microstructure plays an extremely important role in determining the properties of Cr-Mo steels.

The properties of 2¼wt.%Cr-1%Mo steels have been examined extensively in the open literature and in many internal company reports, and additional citing of those research studies is beyond the scope of this paper. However, microstructure and its transformation during heat treatment are extremely important in determining the properties of Cr-Mo steels. More recently, the roles of cooling rate, hardenability, alloying, and microstructure types such as carbide-free acicular bainite and granular bainite on the impact toughness of 2.25Cr-2W(V) steel and high-chromium (9-12Cr) steels (Ref 1) as well as the fracture behavior of bainitic 2.25Cr-2W(V) steels (Ref 2) were determined. The prediction of bainite transformation in 2¼Cr-W steels (Ref 3) and residual stress in 2¼Cr-1Mo steels (Ref 4) during cooling of weldments has been determined. The influence of microstructure and tempering on the hydrogen embrittlement resistance of 2¼Cr-1Mo and 9Cr-1Mo steels was also determined (Ref 5). Finally, the effects of alloy content and cooling rate on thick-walled 1¼Cr-0.5Mo steel vessels were investigated and optimized using thermodynamic prediction software, dilatometry, and mechanical testing (Ref 6).

The effects of molybdenum, chromium, manganese, silicon, carbon, and phosphorus on the resistance of 2¼Cr-1Mo steels to hydrogen and temper embrittlement were determined in earlier studies performed at the former Westinghouse Research and Development Center in Pittsburgh, PA (Ref 7-10). In those studies, a statistically well-designed matrix of thirty-two test steels containing 0.03-0.2%C, 0.1-1.1%Mn, 0.05-0.9%Si, 0.8-3.5%Cr, and 0.3-1.6%Mo was cast, forged, and heat-treated, with some of these steels serving as the raw materials for this study.

A continuous cooling transformation (CCT) diagram is one of the most important tools for predicting microstructural transformation in steel. CCT diagrams are important for designing new alloys in a steel system, or understanding the effects of a heat treatment. Accordingly, CCT diagrams have been published for Cr-Mo steel (Ref 6, 11-15). For example, most recently CCT diagrams were used to evaluate the ability of bainite in a modern TRIP steel to affect the final combination of properties as a function of the bainite volume fraction, steel composition, and component size (Ref 16). However, the CCT characteristics of the important 2¼Cr-1Mo alloy system have never been determined systematically as a function of alloy content.

The cooling rates at which polygonal ferrite is obtained are especially important in the proper design of new Cr-Mo steel alloys. The purpose of the present investigation was to use dilatometry and metallography to develop CCT diagrams for specimens of eight alloys.

The dilatometry as well as its associated metallography and macrohardness were conducted under the direction of the principal author at the former Climax Molybdenum Company in 1985, but the work was never published. For the first time, this paper by all the present authors describes the systematic determination and statistical analysis of the effects of carbon,

John M. Tartaglia, Alison N. Kuelz, and **Veronica Hatty Thelander**, Element Materials Technology, Wixom, MI. Contact e-mail: john.tartaglia@element.com.

manganese, chromium, and molybdenum on 2¼Cr-1Mo CCT diagrams.

2. Experimental Procedure

2.1 Alloy Design and Compositions

Alloying element levels for the statistical design of the original Westinghouse study (Ref 7-10) were based on the ASTM A387 specifications and commercial A387 heats provided by the American Petroleum Institute (API). Eight steels out of the thirty-two Westinghouse steels, a quarter of a 2^6 replicate, were selected for this CCT study. The eight steels contained a constant level of Si and the low (L) and high (H) levels of C, Mn, Cr, and Mo with the P level randomly distributed between L and H. The effects of Si and P on CCT behavior were considered minor and thus not of interest.

The compositions of the eight test steels, as determined by Westinghouse, are shown in Table 1. The molybdenum, manganese, and phosphorus contents were measured by colorimetric methods, the chromium content by a titrimetric method, the silicon content by a gravimetric method, and the carbon content by a combustometric method. In addition, two of the thirty-two original Westinghouse steels contained 10 and 12 ppm As, 1 and 5 ppm Sb, and 5 and 6 ppm Sn.

2.2 Casting

The procedures used for preparation of the Westinghouse laboratory heats have been described in detail (Ref 7, 10). The description is condensed slightly for the purposes of this publication.

The basic iron melting stock had a nominal composition 0.004 wt.%C, 0.002%Si, 0.004%Mn, 0.002%P, and 0.027%Ni. This iron was deoxidized in a flowing dry hydrogen atmosphere for 2 h at 1150 °C (2100 °F) and held in a vacuum until it was used for melting. The iron and iron–phosphorus charge was melted under vacuum at approximately 1625 °C (2930 °F). The furnace power was immediately reduced after meltdown, the furnace was backfilled with helium, and alloying elements were added in the order Cr, Mo, Si, C, and Mn. All alloying additions were high-grade commercial purity materials, including the iron–phosphorus, and excesses of Mn and C were added in order to compensate for normal melting losses. The power was adjusted at each alloying step to compensate for exothermic reactions, especially with C and Mn. The molten bath was then held for 4 min prior to casting into 29-kg (65 lb) ingots. The ingots were 305-mm (12 in.) long tapered square in cross section with side dimensions of approximately 125 mm (5 in.) at the top and 100 mm (4 in.) at the bottom.

2.3 Forging

The hot tops were removed from tapered square ingots prior to forging, leaving ingot sections approximately 250 mm (10 in.) in length by approximately 125 mm (5 in.) at the top and 100 mm (4 in.) at the bottom. The forging temperature was between 1100 and 1200 °C (2010 and 2190 °F). In the first stage of forging, the ingots were reduced to 90-mm (3.5 in.) square in cross section. The 430-460 mm (17-18 in.) long ingots were then sectioned into 140-mm (5.5 in.) pieces, which were then upset in the second stage of forging to 60 mm (2.25 in.) thick by 140-mm (5.5 in.) square. The forged material showed a uniform structure throughout the cross sections.

Table 1 Actual compositions of steels used in this study, wt.%

Steel no.	C	Mn	Cr	Mo	Si	P	C	Mn	Cr	Mo
2	0.17	0.85	2.78	1.27	0.24	0.009	H	H	H	H
3	0.17	0.33	2.73	0.62	0.26	0.022	H	L	H	L
4	0.071	0.37	1.53	0.63	0.26	0.009	L	L	L	L
8	0.069	0.86	1.46	1.29	0.24	0.020	L	H	L	H
11	0.07	0.33	2.69	1.29	0.25	0.010	L	L	H	H
14	0.17	0.36	1.46	1.25	0.26	0.021	H	L	L	H
15	0.072	0.91	2.78	0.63	0.28	0.021	L	H	H	L
32	0.16	0.86	1.46	0.62	0.27	0.009	H	H	L	L

The levels of L and H correspond to the low and high levels of the indicated elements

Table 2 Assorted data of steels of this study, prior to homogenizing

Steel no.	Tempering temperature, °C (°F)	Tempering time, h	Hardness after tempering, HRC	Polygonal ferrite content, %	Prior austenite ASTM grain size no.
2	649 (1200)	2	20	0	7.5
3	607 (1125)	4	19	0	7.0
4	607 (1125)	2	6	20	6.5
8	None	None	23	20	8.75
11	593 (1100)	4	23	5	8.5
14	705 (1300)	2	19	0	7.5
15	593 (1100)	4	23	0	7.5
32	593 (1100)	2	22	0	6.75

Table 3 Critical temperatures, °C

Steel no.	C	Mn	Cr	Mo	Heating cycle	Tc	Ac1	Ac3
2	H	H	H	H	600 → 960(a)	752	785	868
3	H	L	H	L	600 → 960	753	788	865
4	L	L	L	L	600 → 1050(a)	753	775	924
8	L	H	L	H	600 → 1050(a)	760	765	963
11	L	L	H	H	600 → 1050	755	800	945
14	H	L	L	H	600 → 960	755	770	900
15	L	H	H	L	600 → 960	750	785	905
32	H	H	L	L	600 → 960	750	760	875
Ref 11	0	0	0	0		730-740	750-780	880

(a)Averages of multiple heating cycles

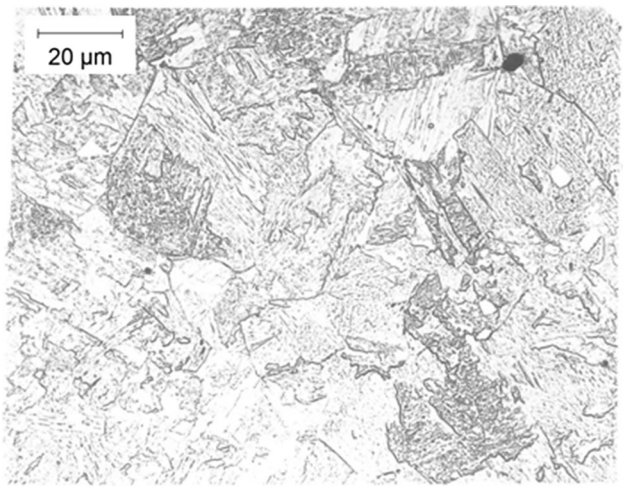

Fig. 1 Optical micrograph of heating cycle specimen of steel 4 quenched from an intercritical temperature of 915 °C

2.4 Heat Treatment and Starting Condition for Dilatometry

Westinghouse heat treated the forgings to form a fully bainitic structure throughout the cross section where compositionally possible. Austempering conditions were selected to avoid transforming to ferrite at the center of the forgings and to avoid transformation to martensite (with the exception of a thin surface layer). The forgings were austenitized at 925 °C (1700 °F) for 2 h, air-cooled to 870 °C (1600 °F) in about 100 s, oil-quenched in about 45 s to approximately 600 °C (1100 °F), transferred to a furnace at 425 °C (800 °F), held for 2 h after they reached 425 °C (800 °F), and air-cooled. The samples supplied for dilatometry were also tempered. The tempering conditions, Rockwell C hardness values (converted from Rockwell B hardness per ASTM E140 where necessary), polygonal ferrite contents, and prior austenite grain sizes (determined by the linear intercept method in accordance with ASTM E112) are shown in Table 2.

Fractured Charpy impact specimens were the starting stock for dilatometer specimens. Two dilatometer specimens were machined from each mating half of a fractured Charpy V-notch specimen. Eleven or twelve specimens with the dimensions

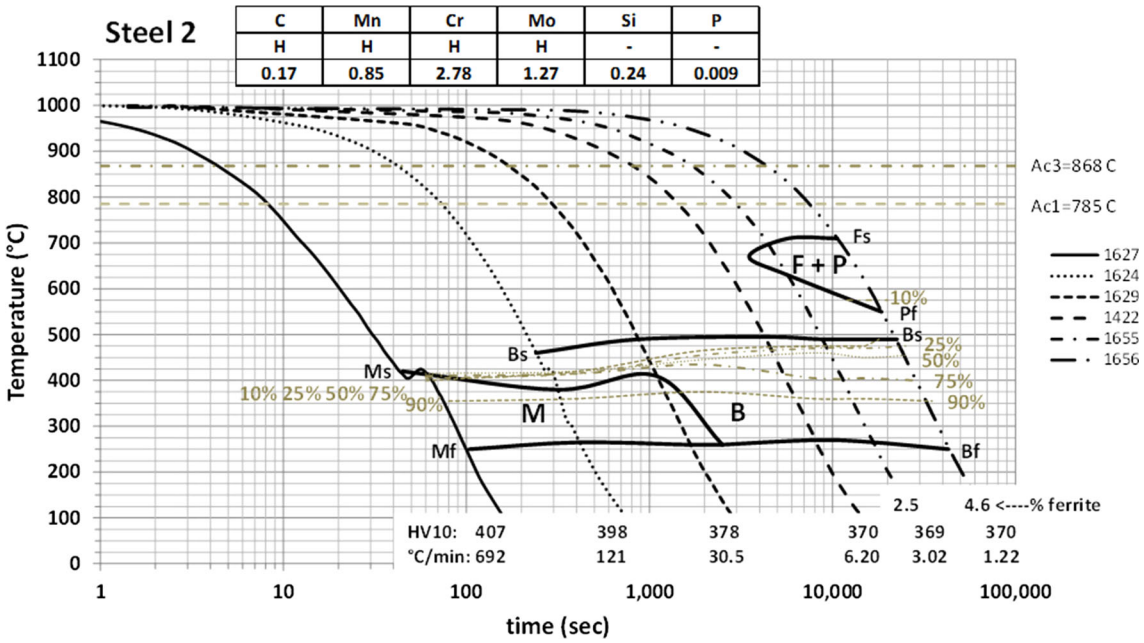

Fig. 2 CCT diagram for steel 2

5 mm (0.197 in.) outside diameter, 3 mm (0.118 in.) inside diameter, and 10 mm (0.394 in.) length were machined for each of the eight steel alloys. After critical temperatures were determined, the remaining dilatometer specimens were encapsulated in individual fused quartz tubes and homogenized. The homogenizing treatment consisted of homogenizing in a box furnace at 1100 °C (2010 °F) for 1 h at temperature followed by air cooling.

2.5 Dilatometry

Dilatometry was conducted with an MMC quenching dilatometer, which is a device that measures the change in length in a metallic specimen as a function of a precisely applied thermal cycle. A record of specimen length versus time, temperature versus time, and specimen length versus temperature is obtained. Critical and transformation temperatures are determined by noting the deviations from normal thermal expansion and contraction behavior.

The critical temperatures were determined for each alloy in the austempered and tempered condition. The specimens were induction heated in the MMC dilatometer at a rapid rate to 600 °C (1100 °F) and then at a rate of 2 °C/min (3.6 °F/min) to a temperature between 960 and 1050 °C (1760 and 1920 °F). Multiple heating cycles were performed for selected alloys, and selected specimens were homogenized in the dilatometer prior to the critical temperature determination. Selected heating cycle specimens were held for 5 min at an intercritical temperature

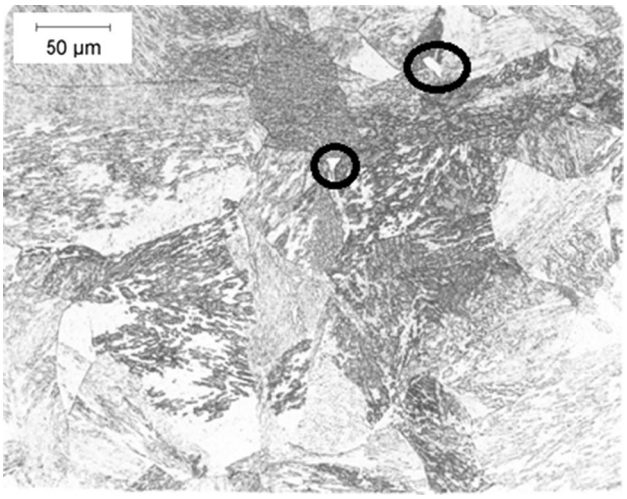

Fig. 3 Optical micrograph of a CCT specimen of steel 2 (CMnCrMo=HHHH) cooled at 3.02 °C/min with hardness of 369 HV10 and ferrite content of 2.5%

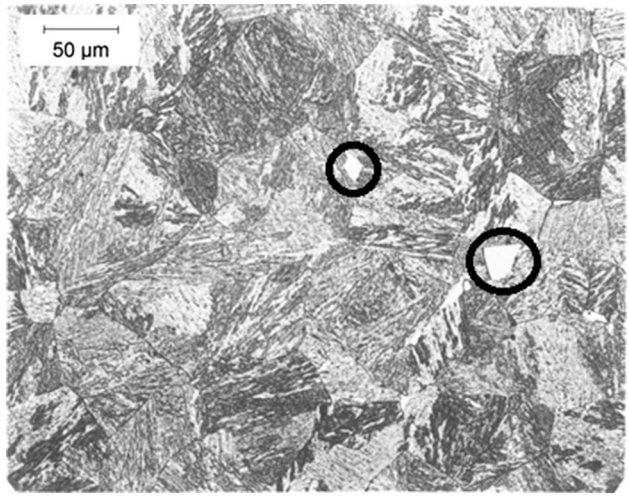

Fig. 5 Optical micrograph of a CCT specimen of steel 3 (CMnCrMo=HLHL) cooled at 30.5 °C/min with hardness of 334 HV10 and ferrite content of 1.6%

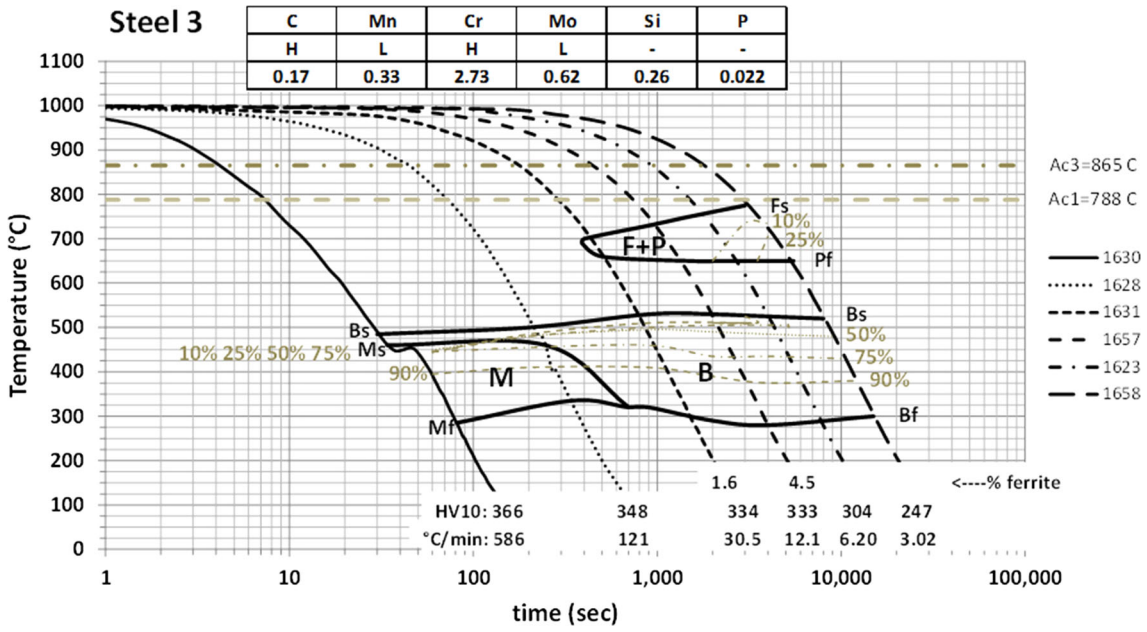

Fig. 4 CCT diagram for steel 3

and cooled at 15,240 °C/min (27,340 °F/min).

A partial continuous cooling transformation (CCT) diagram was constructed for each alloy using MMC dilatometric data in conjunction with metallographic observations and hardness measurements. The homogenized specimens were austenitized in the dilatometer at 1000 °C (1830 °F) for 20 min and radiation cooled or forced convection cooled by helium at selected cooling rates between 1 and 762 °C/min (1.8 and 1370 °F/min). All cooling rates shown in this paper were calculated as average rates of cooling between 800 and 500 °C (1470 and 930 °F).

The ferrite nose cooling rate in a CCT diagram is defined as the maximum cooling rate at which transformation to polygonal ferrite is expected. In this study, the ferrite nose cooling rate was determined as 10% faster than the fastest cooling rate where a small amount of ferrite was found. In seven steels, this "small" amount of ferrite was less than 4.2%; in one steel, this "small" amount of ferrite was 8%.

2.6 Metallography and Hardness

Transverse sections of all CCT specimens were mounted, polished, etched in 4P1N (4 g picric acid, 1 mL nitric acid, and 95 mL ethanol), and photographed with an optical metallograph. The polygonal ferrite content of two CCT specimens per steel was determined by point counting in accordance with ASTM standard E562. The two dilatometer cooling rates per steel that produced the least amount of ferrite were point-counted using a magnification 500 ×, twenty-five (25) fields and a grid with 32 points per field. The Vickers macrohardness (HV10) of each CCT specimen was determined as the average of four readings using a 10-kg load in accordance with ASTM E92.

2.7 Statistical Analysis

Pearson correlation analyses were performed using Minitab® version 15 software. Pearson correlation is a measure of the linear relationship between two or more variables. Correlation coefficients can range from − 1.00 to + 1.00. The *R* value of − 1.00 represents a perfect negative correlation, while a value of + 1.00 represents a perfect positive correlation. An *R* value of 0.00 represents a lack of linear correlation. Pearson correlation coefficients were determined for the lower and upper critical temperatures; the critical cooling rate for ferrite formation; and the martensite-start and martensite-finish temperatures as correlated to the major alloying elements.

Subsequently, multiple linear regression analyses were performed using Minitab® version 15 software to determine equations between those critical temperatures and ferrite content as dependent variables as a function of the major alloying elements as independent variables. In addition to determining regression equations for all the alloying elements, a stepwise regression approach was pursued to eliminate

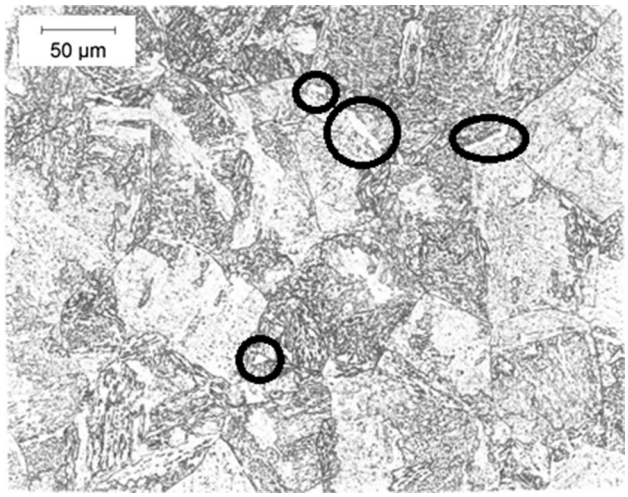

Fig. 7 Optical micrograph of a CCT specimen of steel 4 (CMnCrMo=LLLL) cooled at 508 °C/min with hardness of 223 HV10 and ferrite content of 2.7%

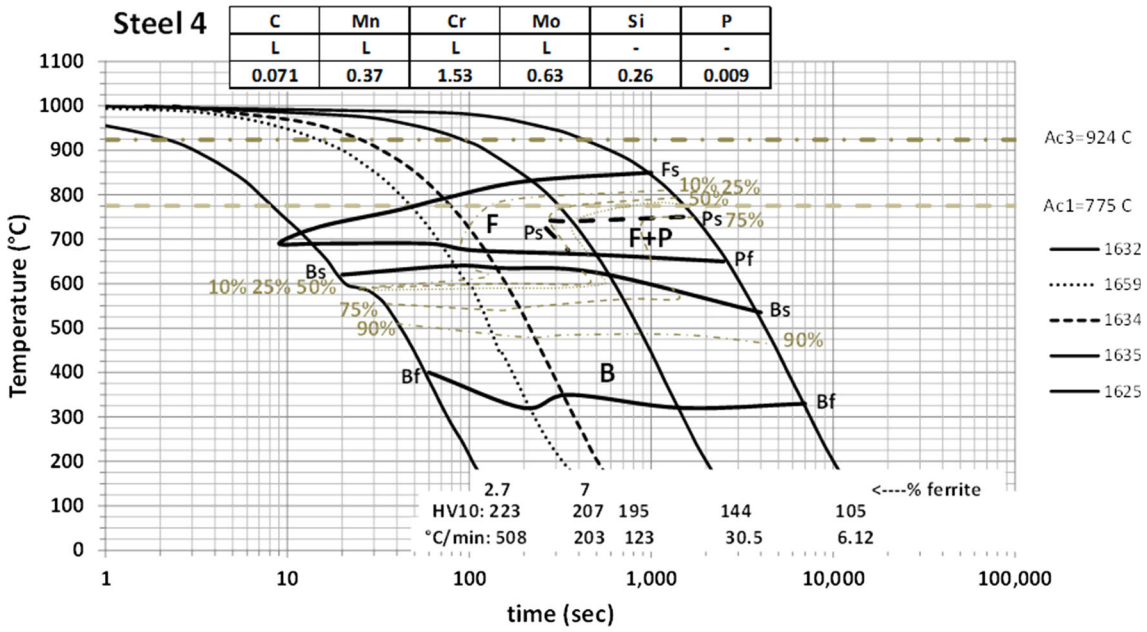

Fig. 6 CCT diagram for steel 4

regression coefficients with relatively high rejection probabilities.

3. Results and Discussion

3.1 Critical Temperatures

For a hypoeutectoid steel (less than about 0.8%C), the lower critical temperature (Ac1) is defined as the temperature at which austenite first forms on heating, and the upper critical temperature (Ac3) is defined as that at which the last ferrite transforms to austenite. Usually, the Ac1 is obtained as the first deviation from linearity upon heating, and the Ac3 is obtained as the point where a second deviation to linearity is obtained. However, previous researchers (Ref 11) have shown that 2¼Cr-1Mo steels exhibit a minute change from linearity termed Tc, before the Ac1 is encountered in a heating curve. These authors further speculated that the observed Tc phenomenon is due to the formation of alloy carbides, or the transformation of one alloy carbide species to another.

The three critical temperatures are shown for each alloy in Table 3. In several cases, for four of the five low-carbon steels, heating to 960 °C (1760 °F) was insufficient to dissolve all the ferrite. Figure 1 shows proeutectoid ferrite in the microstructure (at 200 × original magnification) of a heating cycle specimen that was quenched from an intercritical temperature of 915 °C (1680 °F). Therefore, as a precaution to ensure that all the CCT samples were fully austenitic prior to CCT diagram generation, all the samples were homogenized at 1100 °C (2010 °F) prior to the dilatometer cycle; furthermore, during the CCT cycle itself, the samples were austenitized at 1000 °C (1830 °F).

3.2 Continuous Cooling Transformation Diagrams

Partial continuous cooling transformation (CCT) diagrams followed by one micrograph corresponding to each of the eight alloys are shown in Fig. 2-17. Microstructures were obtained for all cooling rates, but for reasons of brevity, this paper includes only the microstructure corresponding to the fastest cooling rate that produced any polygonal ferrite. The dilatometer run numbers are shown in the plot legends and are keyed to the results listed in Tables 4 and 5, which quantitatively summarize the CCT diagrams. The hardness versus cooling rate for the four low-carbon and four high-carbon steels is also shown in Fig. 18(a) and (b), respectively.

All optical micrographs were obtained after etching with 4P1N and with an original magnification of 200 ×. The polygonal ferrite contents for selected CCT specimens are shown in Table 4. The polygonal ferrite is circled in the micrographs.

The CCT diagrams and micrograph captions also show the low (L)/high (L) designation for the C, Mn, Cr, and Mo

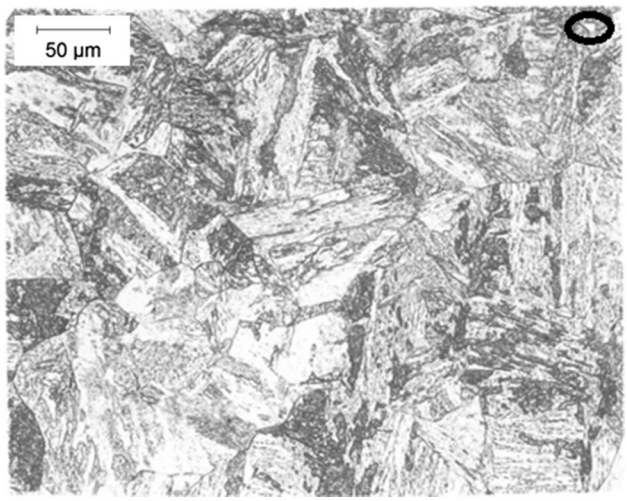

Fig. 9 Optical micrograph of a CCT specimen of steel 8 (CMnCrMo=LHLH) cooled at 121 °C/min with hardness of 267 HV10 and ferrite content of < 1%

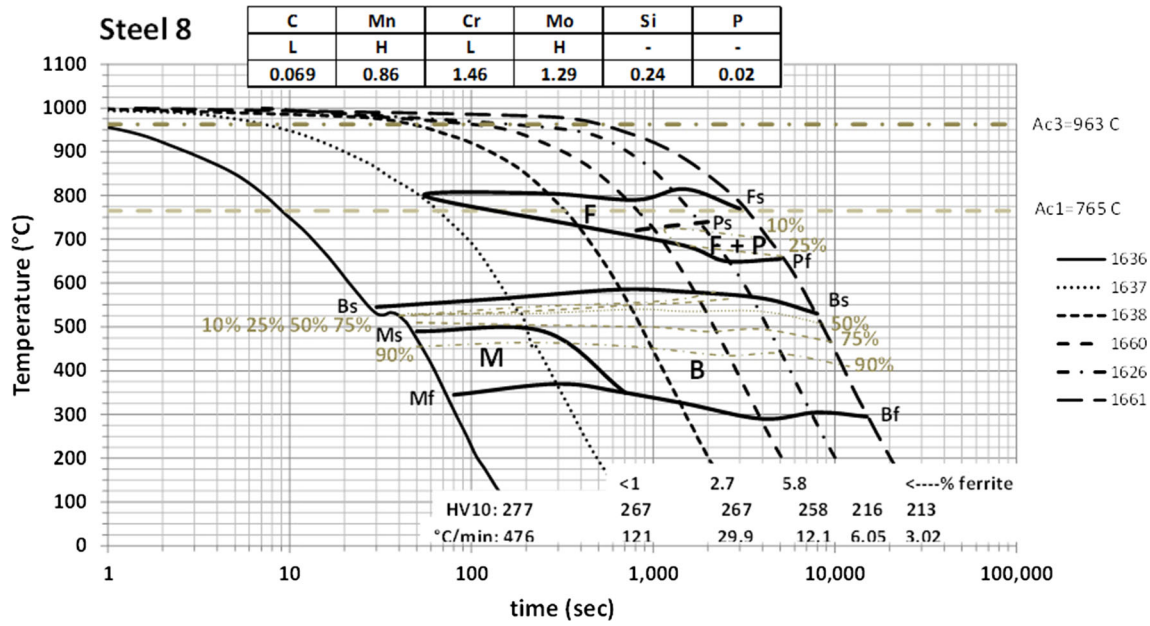

Fig. 8 CCT diagram for steel 8

alloying element levels. The ferrite content, cooling rates, and Vickers macrohardness are also shown at the base of each cooling curve in the CCT diagrams and in the figure captions of each optical micrograph. The transformation regions are labeled with capital letters for polygonal ferrite (F), pearlite (P), bainite (B), and martensite (M). The start and finish temperatures for the transformation regions are identified by the capital letter subscripted with an "s" or "f," respectively. The percentage of austenite transformed is labeled in each transformation region.

The greatest qualitative differences in the CCT diagrams were between those corresponding to the low-carbon alloys (see Fig. 6, 8, 10, and 14) versus the high-carbon alloys (see Fig. 2, 4, 12, and 16). In most of the low-carbon alloys:

- Martensite was completely absent
- Ferrite and bainite were present at almost all cooling rates
- Mostly bainite was present at fast cooling rates
- Mostly ferrite and pearlite were present at slow cooling rates
- Bainite-start and martensite-start temperatures were higher than those of the high-carbon alloys

In most of the high-carbon alloys:

- Hardness values at the faster cooling were greater than for the low-carbon alloys, but hardness similar to the low-carbon alloys was observed at the slower cooling rates
- Mostly bainite with some martensite was present at fast cooling rates
- Mostly bainite with some ferrite was present at slow cooling rates.

3.3 Pearson Correlation Analysis

The results of the Pearson correlation analysis are shown in Table 6 for various parameters on the CCT diagrams. Both the Pearson correlation coefficient (R) and the rejection probability (p) are shown for each of the dependent variables of lower and upper critical temperatures for the eight cases shown in Table 3. For the forty-six cases shown in Table 5, the R and p values are also shown for the bainite-start and bainite-finish temperatures, as well as the martensite-start and martensite-finish temperatures as a function of the independent variables, i.e., the four alloying elements C, Mn, Cr, and Mo. For conditions in Table 6, values that show R values below ± 0.5 or rejection probabilities greater than 0.1 (10%) are italicized because there was insufficient linear correlation between the dependent and independent variables; conversely, significant Pearson coefficients with rejection probabilities below 0.1 (10%) are emboldened. Other complex relationships (higher-order and cross-element terms) may exist, and future statistical analyses could be performed to determine them.

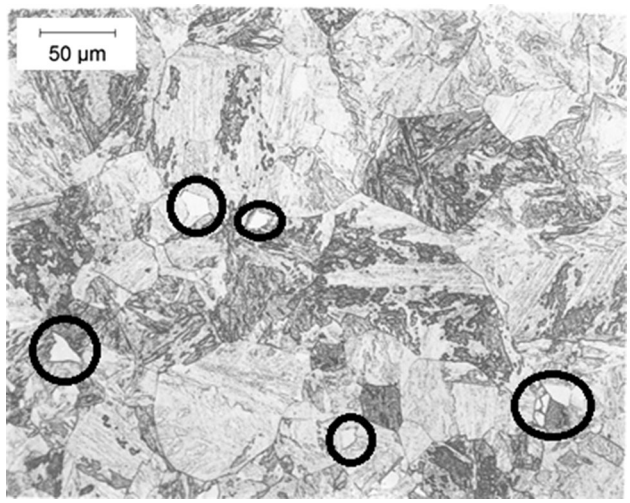

Fig. 11 Optical micrograph of a CCT specimen of steel 11 (CMnCrMo=LLHH) cooled at 115 °C/min with hardness of 296 HV10 and ferrite content of 3.8%

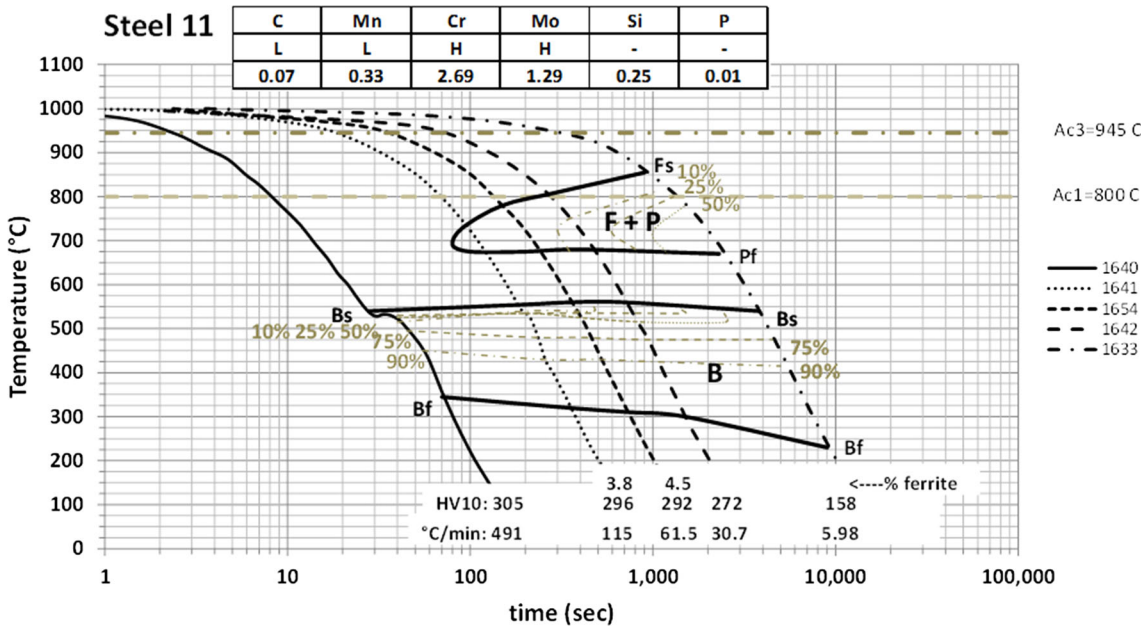

Fig. 10 CCT diagram for steel 11

By definition from the iron–carbon phase diagram, the lower critical temperature is constant with respect to carbon content at 723 °C (1333 °F) so no Pearson coefficient is applicable as a function of carbon content. Also, no investigation of heating rate was investigated, which was "infinitely slow" so the critical temperatures are also listed as "not applicable."

The Pearson correlation analysis found that increasing carbon content had a significant effect on decreasing the upper critical temperature, as expected from the iron–carbon phase diagram. Furthermore, increasing chromium content significantly increased the lower critical temperature.

The Pearson correlation analysis found that increasing chromium content had a significant effect on decreasing the bainite-start, bainite-finish, martensite-start, and martensite-finish temperatures. Increasing carbon content significantly decreased the bainite-start, ferrite-start, and martensite-finish temperatures.

Table 7 shows the approximate critical cooling rate for ferrite formation determined for the eight steels of this study. Using those values, the results of the Pearson correlation analysis for the eight cases are shown in Table 8. The Pearson correlation coefficients were determined for the alloying elements versus the ferrite nose cooling rate, i.e., the critical cooling rate for ferrite formation (CCRF), which was determined as 10% faster than the fastest cooling rate where a small amount of ferrite was found. For all the variables in the table, the rejection probabilities were greater than 0.1 (10%) and are italicized because there was insufficient correlation between the dependent and independent variables. However, when a Pearson correlation analysis of the logarithm of the CCRF was measured for the alloying elements, Table 8 shows a highly negative correlation between the log CCRF and the carbon content.

3.4 Multiple Regression Analysis

The results of the multiple regression analysis are shown in Table 9 for various parameters on the CCT diagrams. Table 9 contains both the regression coefficient and the rejection probability (p) for each of the dependent variables of lower and upper critical temperatures for the eight cases shown in Table 3. For the forty-six cases shown in Table 5, Table 9 also contains the regression coefficients and p values for the bainite-start and bainite-finish temperatures, as well as the martensite-start and martensite-finish temperatures as a function of the independent variables, i.e., the four alloying elements C, Mn, Cr, and Mo.

The authors used stepwise regression and the rejection probability ($P > 0.1$) to eliminate alloying elements as independent variables from the regression. Furthermore, the overall coefficient of determination ($R^2 > 0.7$) was used to select the best form of the regression equation, if any. It is important to

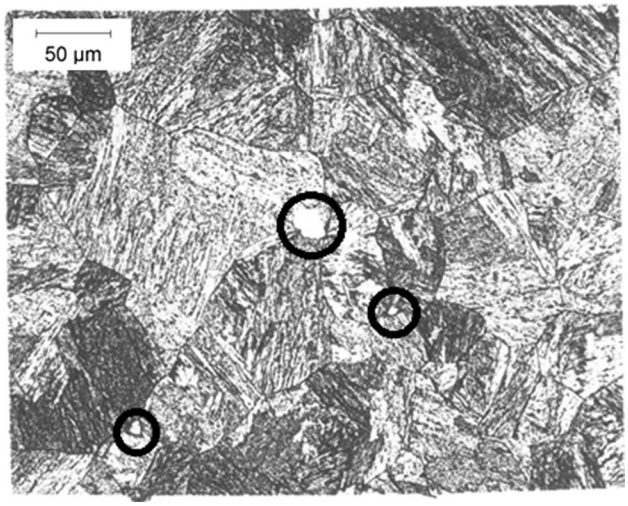

Fig. 13 Optical micrograph of a CCT specimen of steel 14 (CMnCrMo=HLHL) cooled at 12.1 °C/min with hardness of 295 HV10 and ferrite content of 4.2%

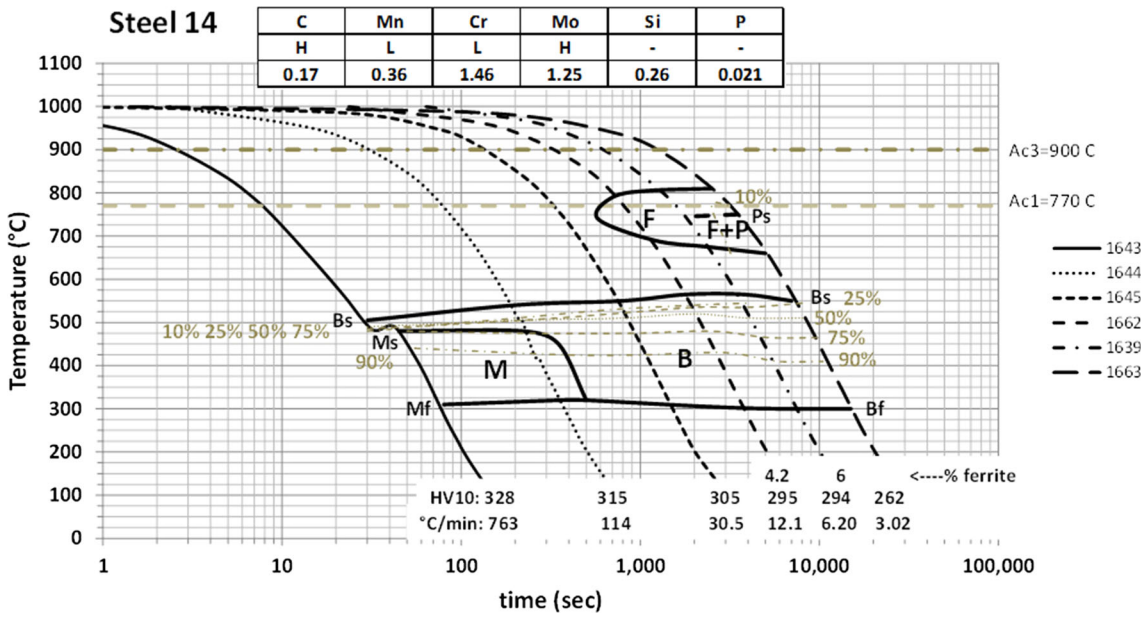

Fig. 12 CCT diagram for steel 14

emphasize that if R^2 values decreased after eliminating coefficients, those regression equations with fewer terms were also italicized to their "All Possible Variables" counterparts. Keeping single element coefficients in a simple regression equation was also an overriding consideration; this is a common technique for hardenability regression analyses, as done in other studies (Ref 6, 17).

The authors investigated many complex relationships (with cross-element independent variable terms such as CxCr and different CCT parameters as dependent variables such as the start and finish temperatures). Some of these relationships attempts are listed in Table 9.

The present investigators evaluated the time to ferrite-start in the manner pursued by earlier investigators (Ref 6), but Tables 8 and 9 show that low Pearson correlation coefficients and no regression equation with a reasonable R^2 value were found for this and for most parameters. Based on the modeling performed by earlier authors (Ref 11), the current authors investigated the relationship between alloying elements and the logarithm of the critical cooling rate for ferrite formation (log CCRF). The present authors obtained the following equation and reasonable validity (see Table 9) for the log CCRF regression equation:

$$\text{Log}_{10}\text{CCRF}\ (^{\circ}\text{C/minute}) = -10.2\ \text{C} - 0.94\ \text{Mn} - 0.34\ \text{Cr} - 0.57\ \text{Mo} + 4.7$$

As shown in Table 9, in this study, the present authors also obtained the following regression equations with reasonable validity for the lower critical temperature (Ac1) and upper critical temperature (Ac3):

$$\text{Ac1}\ (^{\circ}\text{C}) = -18.5\ \text{Mn} + 17.3\ \text{Cr} + 5.1\ \text{Mo} + 748$$
$$\text{Ac3}\ (^{\circ}\text{C}) = -582.4\ \text{C} - 14.8\ \text{Cr} + 41.9\ \text{Mo} + 966$$

Just these three equations alone represent a significant contribution to the metallurgical community in the design of new steels in the 2¼Cr-1Mo field and for altering alloy content to perform proper heat treatments and avoid ferrite formation in large 2¼Cr-1Mo components.

3.5 Agreement with Previous Studies

The critical temperatures and critical cooling rate for ferrite formation were determined by Eldis and Wada (Ref 11) for three steels that were essentially centered between the H and L values in Table 1 for the compositions of this study. Table 3 shows satisfactory agreement for the present results with the critical temperatures determined in the earlier study. However, Table 7 shows satisfactory agreement for only the high-carbon steels because ferrite was obtained for almost all the cooling rates for the low carbon heats of this study.

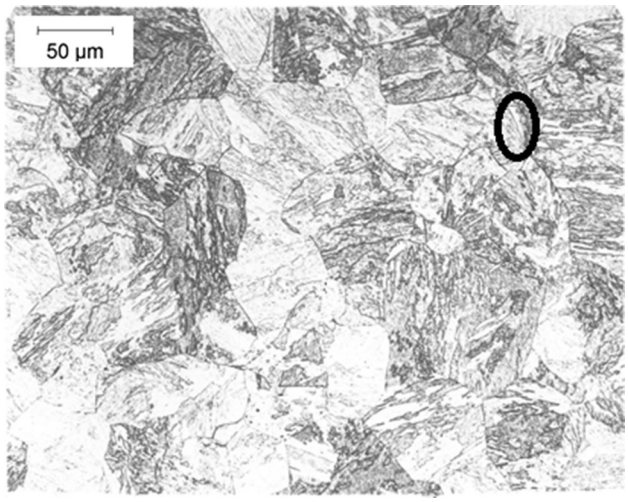

Fig. 15 Optical micrograph of a CCT specimen of steel 15 (CMnCrMo=LHHL) cooled at 30.5 °C/min with hardness of 297 HV10 and ferrite content of < 1%

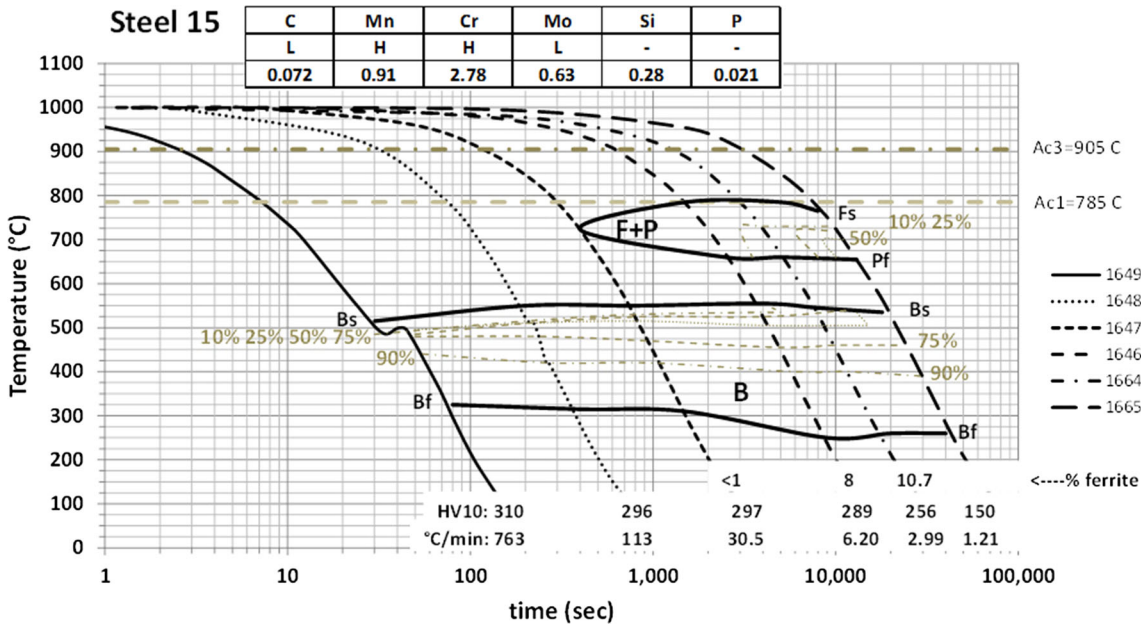

Fig. 14 CCT diagram for steel 15

An R value of 0.9 is equivalent to an R^2 value of 0.8, which means that a regression equation explains 80% of the variance while 20% of the variation is due to error. Obtaining an R^2 value greater than 0.9 is always desirable, but only the Ac3 equation achieved this objective, and no confounded variables or more complex regression were obtained. Only eight steels were evaluated without any duplicate readings. Therefore, the authors consider the respective R^2 values of 0.89 and 0.83 for the Ac1 and log CCRF equations more than adequate because greater than 83% of the variance is explained by the data and only 17% is attributable to random error. As a point of comparison, the Eldis (Ref 17) equations had R^2 values of 0.86 and 0.71 and the Trzaska (Ref 18) equations had R^2 values of 0.50 and 0.72 for their Ac1 and Ac3 equations, respectively. Consequently, the R^2 values for the present study's equations compare quite favorably with the significance of these prior authors' equations.

Many investigators, including Eldis (Ref 17), have determined regression equations for the martensite-start (Ms) temperature as a function of alloy content. These equations show that increasing concentrations of austenite-stabilizing elements including carbon, manganese, and nickel decrease the Ms temperature. This study was probably unsuccessful in achieving a reasonable R^2 value for an Ms temperature because there was only limited applicable results, i.e., these steels were nickel-free and only the four high-carbon steels formed martensite and exhibited an Ms temperature.

Eldis (Ref 17) determined the effect of composition and the following regression equations:

$$\begin{aligned}\text{Ac1}\,(^\circ\text{C}) &= 20.1\,\text{Si} - 17.8\,\text{Mn} - 9.8\,\text{Mo} + 11.9\,\text{Cr} \\ &\quad - 19.1\,\text{Ni} + 712 \\ \text{Ac3}\,(^\circ\text{C}) &= -254.4\,\text{C} + 51.7\,\text{Si} - 14.2\,\text{Ni} + 871\end{aligned}$$

on a wide variety of 174 alloy steels with 0.1-0.8%C, 0.2-1.5%Si, 0.4-1.8%Mn, 0-0.9%Mo, 0-1.6%Cr, and 0-4.6%Ni.

Trzaska and Dobrzanski (Ref 18) reviewed the work of several authors and determined the critical temperatures for 200 steels with 0.11-0.77 °C, 0.2-1.53%Mn, 0.14-1.37%Si, 0-1.54%Cr, 0-1.72%Ni, 0-0.72% Mo, 0-0.31%V, and 0-0.26%Cu. They published the following regression equations:

$$\begin{aligned}\text{Ac1}\,(^\circ\text{C}) &= 739.3 - 22.8\,\text{C} - 6.8\,\text{Mn} + 18.2\,\text{Si} \\ &\quad + 11.7\,\text{Cr} - 15\,\text{Ni} - 6.5\,\text{Mo} - 5\,\text{V} - 28\,\text{Cu} \\ \text{Ac3}\,(^\circ\text{C}) &= 937.3 - 224.5\,\text{C}^{0.5} - 17\,\text{Mn} + 34\,\text{Si} \\ &\quad - 14\,\text{Ni} + 21.6\,\text{Mo} + 41.8\,\text{V} - 20\,\text{Cu}\end{aligned}$$

Also, Wada and Eldis (Ref 11) determined the effect of composition on the critical cooling rate for ferrite formation, in three 2¼ Cr-1Mo steels with the following regression equation:

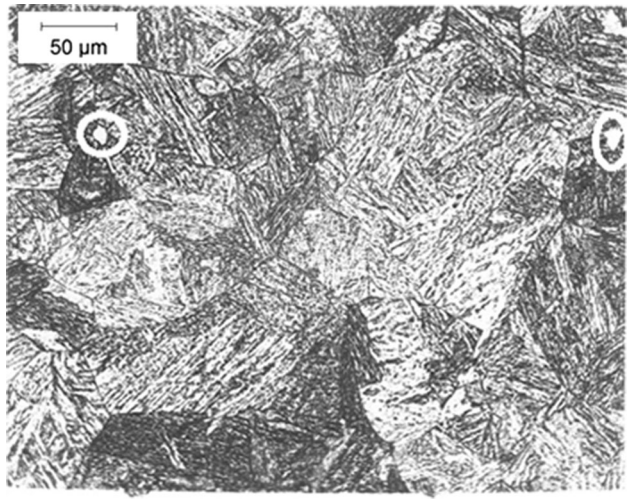

Fig. 17 Optical micrograph of a CCT specimen of steel 32 (CMnCrMo=HHLL) cooled at 30.5 °C/min with hardness of 285 HV10 and ferrite content of 1.6%

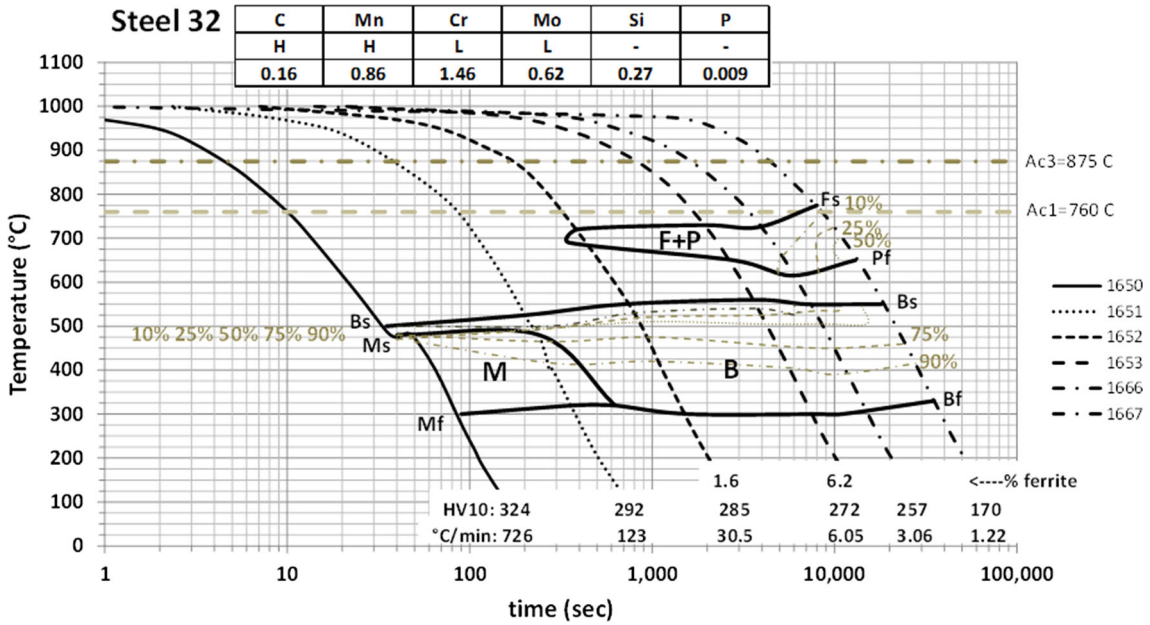

Fig. 16 CCT diagram for steel 32

Table 4 Macrohardness and ferrite content results for the CCT specimens

Steel#	Levels of CMnCrMo	Dilatometer run #	Cooling rate, °C/min	Macrohardness, HV10	Mean ferrite content, %	± 95% confidence interval
2	HHHH	1627	692	407		
2	HHHH	1624	121	398		
2	HHHH	1629	30.5	378		
2	HHHH	1422	6.20	370		
2	HHHH	1655	3.02	369	2.5	0.99
2	HHHH	1656	1.22	370	4.6	1.45
3	HLHL	1630	586	366		
3	HLHL	1628	121	348		
3	HLHL	1631	30.5	334	1.6	0.99
3	HLHL	1657	12.1	333	4.5	1.40
3	HLHL	1623	6.20	304		
3	HLHL	1658	3.02	247		
4	LLLL	1632	508	223	2.7	1.07
4	LLLL	1659	203	207	7.0	1.76
4	LLLL	1634	123	195		
4	LLLL	1635	30.5	144		
4	LLLL	1625	6.12	105		
8	LHLH	1636	476	277		
8	LHLH	1637	121	267		
8	LHLH	1638	29.9	267	2.7	1.01
8	LHLH	1660	12.1	258	5.8	1.72
8	LHLH	1626	6.05	216		
8	LHLH	1661	3.02	213		
11	LLHH	1640	491	305		
11	LLHH	1641	115	296	3.8	1.13
11	LLHH	1654	61.5	292	4.5	1.63
11	LLHH	1642	30.7	272		
11	LLHH	1633	5.98	158		
14	HLHL	1643	763	328		
14	HLHL	1644	114	315		
14	HLHL	1645	30.5	305		
14	HLHL	1662	12.1	295	4.2	1.34
14	HLHL	1639	6.20	294	6.0	1.70
14	HLHL	1663	3.02	262		
15	LHHL	1649	763	310		
15	LHHL	1648	113	296		
15	LHHL	1647	30.5	297		
15	LHHL	1646	6.20	289	8.0	1.45
15	LHHL	1664	2.99	256	10.7	3.55
15	LHHL	1665	1.21	150		
32	HHLL	1650	726	324		
32	HHLL	1651	123	292		
32	HHLL	1652	30.5	285	1.6	1.75
32	HHLL	1653	6.05	272	6.2	1.75
32	HHLL	1666	3.06	257		
32	HHLL	1667	1.22	170		

$$\text{Log CCRF } (^{\circ}\text{C/min}) = 2.03 - 5\ \text{C}$$

Other investigators (Ref 6) stated that the CCRF was 15-200 °C/min for two 1¼ Cr-0.5Mo steels.

The steels of the present study are nominally within the composition ranges of these earlier authors (Ref 6, 11, 18). Therefore, it is a useful exercise to compare the predictions from the three equations listed in the previous Multiple Regression Analysis section of this paper with the predictions of the equations listed in this section of the paper from the research of these other authors. Table 10 shows such a comparison between the predictions at 25% of the range (0.1%C, 0.25%Si, 0.48%Mn, 0.8%Mo and 1.8%Cr) and 75% of the range (0.15%C, 0.27%Si, 0.77%Mn, 1.1%Mo, and 2.5%Cr) based on the range of elements evaluated in this study (see Table 1). Table 10 exhibits variable quality in the agreement between the predictions from this and earlier studies' regression equations.

Table 5 Transformation start and finish temperatures for the CCT specimens

			Temperature, °C						
			Martensite		Bainite		Ferrite	Pearlite	Ferrite + pearlite
Steel #	Levels of CMnCrMo	Dilatometer run #	Start Ms	Finish Mf	Start Bs	Finish Bf	Start Fs	Start Ps	Finish FPf
2	HHHH	1627	410	250					
2	HHHH	1624	380	265	460	380			
2	HHHH	1629	410	260	490	410			
2	HHHH	1422			495	270			
2	HHHH	1655			490	265	630		630
2	HHHH	1656			490	250	710		550
3	HLHL	1630	460	285	485	460			
3	HLHL	1628	460	335	500	460			
3	HLHL	1631			530	320	690		690
3	HLHL	1657			530	290	730		650
3	HLHL	1623			525	280	750		675
3	HLHL	1658			520	300	775		650
4	LLLL	1632			620	400	728		728
4	LLLL	1659			640	320	765		690
4	LLLL	1634			635	350	790		675
4	LLLL	1635			625	320	830	740	665
4	LLLL	1625			535	330	850	750	650
8	LHLH	1636	490	345	545	490			
8	LHLH	1637	490	370	565	490			
8	LHLH	1638			585	325	805		730
8	LHLH	1660			580	290	790	720	685
8	LHLH	1626			565	305	815	740	650
8	LHLH	1661			530	295	770		655
11	LLHH	1640			540	345			
11	LLHH	1641			555	320	728		728
11	LLHH	1654			560	310	780		675
11	LLHH	1642			560	300	810		680
11	LLHH	1633			540	230	855		670
14	HHLH	1643	480	310	505	480			
14	HHLH	1644	480	320	540	480			
14	HHLH	1645			550	300			
14	HHLH	1662			565	305	740		740
14	HHLH	1639			565	300	805	745	675
14	HHLH	1663			550	300	810	750	660
15	LHHL	1649			515	325			
15	LHHL	1648			550	315			
15	LHHL	1647			550	310	723		723
15	LHHL	1646			555	250	785		660
15	LHHL	1664			545	260	785		660
15	LHHL	1665			535	260	765		655
32	HHLL	1650	480	300	500	480			
32	HHLL	1651	480	320	525	480			
32	HHLL	1652			550	300	690		690
32	HHLL	1653			560	300	730		650
32	HHLL	1666			550	255	725		615
32	HHLL	1667			550	330	775		650

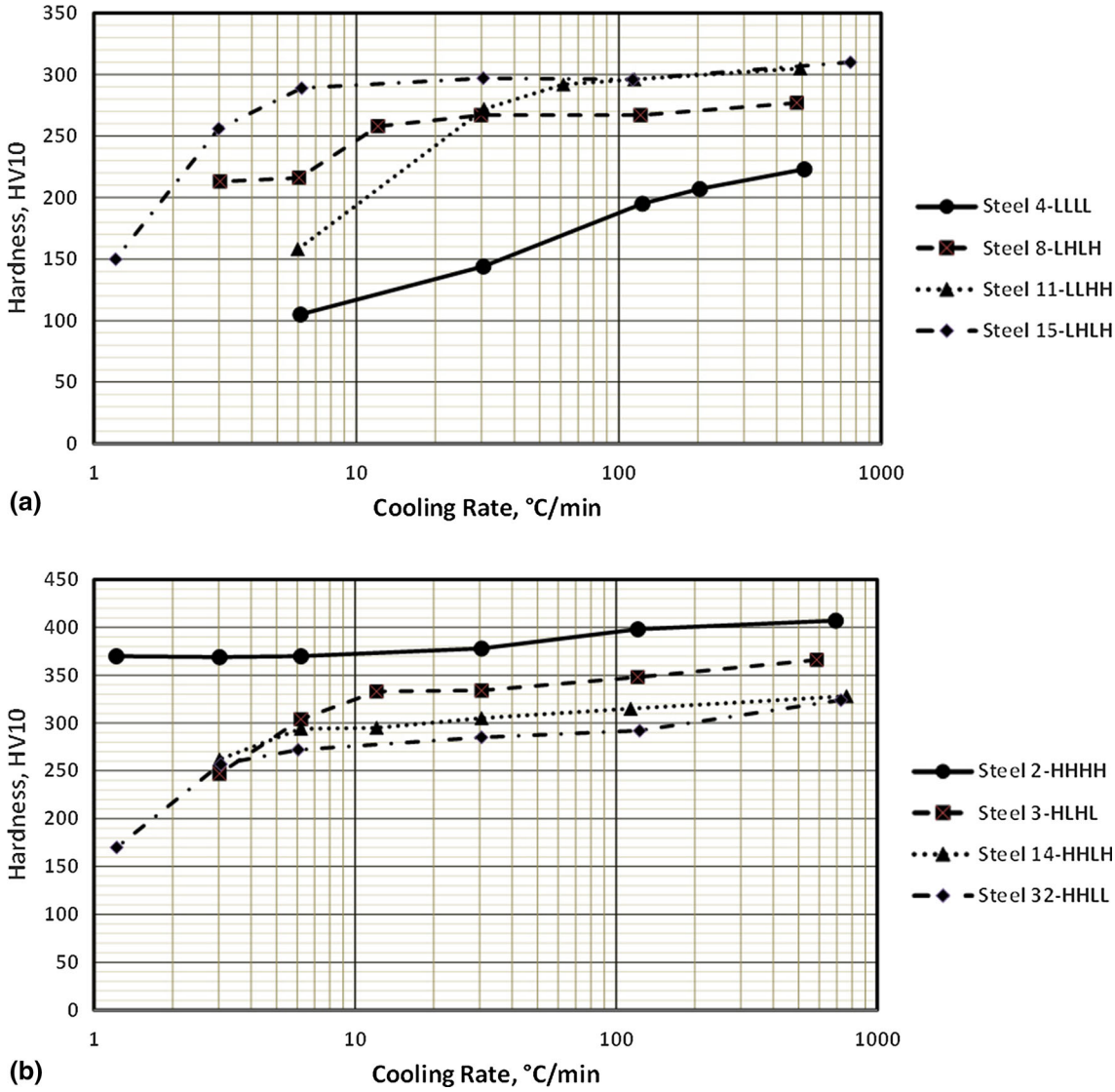

Fig. 18 (a) Hardness vs. cooling rate for low-carbon steels, (b) hardness vs. cooling rate for high-carbon steels

Table 6 Results of the Pearson correlation coefficient analysis on CCT parameters

CCT parameter	Coefficient, *R* Rejection probability (*p*)	# of data points	wt.% of C	Mn	Cr	Mo
Lower critical temperature (Ac1)	*R*	8	NA	*− 0.39*	**0.88**	*0.13*
	(*p*)			*(0.34)*	(0.00)	*(0.76)*
Upper critical temperature (Ac3)	*R*	8	**− 0.85**	*− 0.07*	*− 0.30*	*0.42*
	(*p*)		(0.01)	*(0.86)*	*(0.46)*	*(0.30)*
Martensite-start temperature (Ms)	*R*	12	*− 0.44*	*− 0.33*	**− 0.55**	*− 0.04*
	(*p*)		*(0.15)*	*(0.29)*	(0.06)	*(0.91)*
Martensite-finish temperature (Mf)	*R*	12	**− 0.69**	*− 0.19*	**− 0.55**	*0.04*
	(*p*)		(0.01)	*(0.55)*	(0.06)	*(0.91)*
Bainite-start temperature (Bs)	*R*	45	**− 0.56**	*− 0.22*	**− 0.50**	*− 0.14*
	(*p*)		(0.00)	*(0.15)*	(0.00)	*(0.35)*
Bainite-finish temperature (Bf)	*R*	45	*0.15*	*− 0.07*	**− 0.30**	*0.02*
	(*p*)		*(0.34)*	*(0.65)*	(0.05)	*(0.90)*
Ferrite-start temperature (Fs)	*R*	30	**− 0.51**	*− 0.25*	*− 0.26*	*0.16*
	(*p*)		(0.00)	*(0.18)*	*(0.17)*	*(0.40)*
Pearlite-start temperature (Ps)	*R*	6	*0.47*	*− 0.76*	*0.29*	*− 0.33*
	(*p*)		*(0.34)*	*(0.08)*	*(0.58)*	*(0.53)*
Ferrite + pearlite-finish temperature (FPf)	*R*	30	*− 0.33*	*− 0.30*	*− 0.16*	*0.03*
	(*p*)		*(0.07)*	*(0.11)*	*(0.39)*	*(0.86)*

NA not applicable

Table 7 Critical cooling rate for ferrite formation

Steel #	Levels of CMnCrMo	Critical cooling rate for ferrite formation, °C/min
2	HHHH	3.322
3	HLHL	33.55
4	LLLL	558.8
8	LHLH	133.1
11	LLHH	126.5
14	HHLH	13.31
15	LHHL	33.55
32	HHLL	33.55
Ref 11	0000	46-33

Table 8 Results of the Pearson correlation coefficient analysis on critical cooling rate for ferrite formation

Parameter	Coefficient, *R* Rejection probability (*p*)	# of data points	wt.% of C	Mn	Cr	Mo
Critical cooling rate for ferrite formation (ferrite nose cooling rate) (CCRF)	*R*	16	*− 0.554*	*− 0.354*	*− 0.368*	*− 0.263*
	(*p*)		*(0.154)*	*(0.390)*	*(0.370)*	*(0.530)*
log (CCRF)	*R*	16	**− 0.763**	*− 0.334*	*− 0.365*	*− 0.262*
	(*p*)		(0.028)	*(0.419)*	*(0.375)*	*(0.531)*

Table 9 Results of the multiple regression analysis on CCT parameters

Parameter	Regression type	# of data points	Regression coefficient: Rejection probability (*p*) Constant	C	Mn	Cr	Mo	CxCr	Coefficient of determination, R^2
Lower critical temperature (Ac1)	All possible variables	8	**748.466**	NA	**− 18.486**	**17.251**	**5.123**		0.888
			(0.000)	NA	(0.037)	(0.002)	(0.350)		
	After elimination	*8*	*742.124*			*17.044*			*0.770*
			(0.000)			*(0.000)*			
Upper critical temperature (Ac3)	All possible variables	8	**966.300**	**− 582.350**		**− 14.787**	**41.940**		0.928
			(0.000)	(0.001)		(0.052)	(0.016)		
	After elimination	*8*	*935.300*	*− 587.300*			*42.340*		*0.836*
			(0.000)	*(0.003)*			*(0.046)*		
	After elimination	*8*	*975.218*	*− 353.250*				*− 109.41*	*0.775*
			(0.000)	*(0.000)*				*(0.000)*	
	After elimination	*8*	*976.012*	*− 591.550*					*0.705*
			(0.000)	*(0.000)*					
Martensite-start temperature (Ms)	*All possible variables*	*12*	*666.370*	*− 578.200*	*− 95.680*	*− 24.880*	*− 13.850*		*0.429*
			(0.000)	*(0.119)*	*(0.056)*	*(0.179)*	*(0.675)*		
	After Elimination	*12*	*628.920*	*− 738.100*	*− 98.730*				*0.374*
			(0.000)	*(0.030)*	*(0.050)*				
Martensite-finish temperature (Mf)	*All possible variables*	*12*	*521.700*	*− 809.500*	*− 77.180*	*− 14.030*	*− 16.660*		*0.673*
			(0.000)	*(0.008)*	*(0.028)*	*(0.250)*	*(0.459)*		
	After elimination		*488.240*	*− 874.700*	*− 79.270*				*0.645*
			(0.000)	*(0.001)*	*(0.024)*				
Bainite-start temperature (Bs)	*All possible variables*	*45*	*719.050*	*− 479.450*	*− 46.040*	*− 31.222*	*− 25.770*		*0.672*
			(0.000)	*(0.000)*	*(0.001)*	*(0.000)*	*(0.016)*		
Bainite-finish temperature (Bf)	*All possible variables*	*45*	*393.730*	*216.400*	*− 16.010*	*− 34.900*	*− 0.380*		*0.024*
			(0.000)	*(0.354)*	*(0.709)*	*(0.053)*	*(0.991)*		
Ferrite-start temperature (Fs)	*All possible variables*	*30*	*892.22*	*− 540.300*	*− 58.070*	*− 21.410*	*12.840*		*0.337*
			(0.000)	*(0.002)*	*(0.054)*	*(0.086)*	*(0.587)*		
Pearlite-start temperature (Ps)	*After elimination*	*6*	*754.720*	*22.170*	*− 30.520*	*	*		*0.295*
			(0.000)	*(0.831)*	*(0.212)*	*	*		
Ferrite + Pearlite-Finish temperature (FPf)	*All possible variables*	*30*	*755.110*	*− 279.200*	*− 48.250*	*− 10.960*	*− 2.570*		*0.130*
			(0.000)	*(0.051)*	*(0.063)*	*(0.299)*	*(0.899)*		
Critical cooling rate for ferrite formation (ferrite nose cooling rate), log (CCRF)	All possible variables	8	**4.7053**	**− 10.208**	**− 0.935**	**− 0.341**	**− 0.565**		0.830
			(0.004)	(0.015)	(0.090)	(0.112)	(0.161)		
	After elimination	*8*	*3.43*	*− 10.261*	*− 0.9189*				*0.615*
			(0.001)	*(0.020)*	*(0.167)*				

All alloy contents are in wt.%, and temperatures are in °C

*Minitab automatically removed these variables from this regression equation because Cr and Mo are highly correlated with other independent variables in the limited data available

Table 10 Comparison of parameter prediction between this and earlier (Ref 6, 11, 17, 18) studies

Parameter	Units	Abbreviation	This work	Eldis (Ref 17)	Trzaska and Dobrazanski (Ref 18)	Na et al (Ref 6)	Wada and Eldis (Ref 11)
Comparison for 25% range composition							
Lower critical temperature	°C	Ac1	774	722	754	NA	NA
Upper critical temperature	°C	Ac3	917	860	886	NA	NA
Critical cooling rate for ferrite formation	°C/min	CCRF	169	NA	NA	15-200	36
Comparison for 75% range composition							
Lower critical temperature	°C	Ac1	782	722	757	NA	NA
Upper critical temperature	°C	Ac3	892	848	872	NA	NA
Critical cooling rate for ferrite formation	°C/min	CCRF	11	NA	NA	15-200	20

4. Conclusions

1. The upper critical temperature was decreased significantly by increasing carbon content. The lower critical temperature was increased significantly by increased chromium content.
2. Increasing chromium content had a significant effect on decreasing the bainite-start, bainite-finish, martensite-start, and martensite-finish temperatures. Increasing carbon content significantly decreased the bainite-start, ferrite-start, and martensite-finish temperatures.
3. The following regression equations were obtained in this study:

a. $Ac1\ (°C) = -18.5\ Mn + 17.3\ Cr + 5.1\ Mo + 748$
b. $Ac3\ (°C) = -582.4\ C - 14.8\ Cr + 41.9\ Mo + 966$
c. $Log_{10}\ CCRF\ (°C/min) = -10.2\ C - 0.94\ Mn - 0.34\ Cr - 0.57\ Mo + 4.7$.

Acknowledgments

The authors gratefully acknowledge Bevil J. Shaw for his project activities to provide the source materials at the former Westinghouse R&D Center in Pittsburgh, PA and the permission of R. W. Swindeman of Oak Ridge National Laboratories to utilize the Charpy specimens tested in Department of Energy Contract No. DE-AC05-78ET13513. The authors wish to thank the management and staff of the Climax Molybdenum Company and Westinghouse for funding and performing some of the technical experiments.

References

1. R.L. Klueh, P.J. Maziasz, and D.J. Alexander, Bainitic Chromium-Tungsten Steels with 3% Chromium, *Metall. Mater. Trans. A*, 1997, **28A**(2), p 335–345A
2. R.L. Klueh, D.J. Alexander, and P.J. Maziasz, Fracture Behavior of Bainitic Chromium-Tungsten and Chromium-Molybdenum Steels, in *Proceedings of 36th Mechanical Working and Steel Processing Conference, 16–19 October 1994, Baltimore, Maryland, IIS/AIME*, 1994, p. 443–452
3. M.J. Xu, H. Lu, C. Yu, J.J. Xu, and J.M. Chen, Finite Element Simulation of Butt Welded 2.25Cr-1.6W Steel Pipe Incorporating Bainite Phase Transformation, *Sci. Technol. Weld. Join.*, 2013, **18**(3), p 184–190
4. Y. Luo, D.-A. Deng, and X.-L. Jiang, Prediction of Welding Residual Stress in 2.25Cr-1Mo Steel Pipe, *J. Shanghai Jiaoting Univ. (Sci.)*, 2006, **E-11**(1), p 77–83
5. N. Parvathavarthini, S. Saroja, and R.K. Dayal, Hydrogen Transport in Chrome-Moly Steels and Susceptibility to Hydrogen Embrittlement: Correlation with Microstructure, in *Proceedings of "ISOMALM 2000: International Symposium on Materials Ageing and Life Management, Kalpakkam, India, 3–6 October 2000*, Allied Publishers Lt., New Delhi, 2000, p. 1045–1050
6. H. Na, B. Kim, S. Lee, and C.Y. Kang, Thermodynamic Alloy Design of High Strength and Toughness in 300 mm Thick Pressure Vessel Wall of 1.25Cr-0.5Mo Steel, *Metals*, 2018, **8**, p 70. https://doi.org/10.3390/met8010070
7. B.J. Shaw, *Study to Optimize Cr-Mo Steels to Resist Hydrogen and Temper Embrittlement (WEC-3.2.3)*, Contract No. DE-AC05-78-R13513, U.S. Department of Energy, Division of Coal Conversion, Quarterly Report No. 7, 1980
8. B.J. Shaw and J. Greggi, Study to Optimize Cr-Mo Steels to Resist Hydrogen and Temper Embrittlement (WEC-3.3), in *Fossil Energy Materials Program Quarterly Progress Report, ORNL/FMP-82/4, for the Period Ending September 30,* 1982, p. 123
9. B.J Shaw, Study to Optimize Cr-Mo Steels to Resist Hydrogen and Temper Embrittlement (WEC-3.3), in *Fossil Energy Materials Program Quarterly Progress Report," ORNL/FMP-83/2 for the Period Ending March 31*, 1983, p. 177
10. B.J. Shaw, A Study of Carbides Formed in Low Alloy Cr-Mo Steels, in *Research on Chrome-Moly Steels, MPC-21*, American Society of Mechanical Engineers, New York, 1984, p. 117–128
11. T. Wada, G.T. Eldis, Transformation Characteristics of 2¼Cr-1Mo Steel, in *Application of 2¼ Cr-1Mo Steel for Thick-Wall Pressure Vessels*, G.S. Sangdahl and M. Semchyshen, Ed., American Society for Testing and Materials, 1982, p. 343–362
12. R. Petri, E. Schnabel, and P. Schwaab, On the Influence of the Alloying Elements on the Transformation and Precipitation Processes During Cooling of Creep-Resistant Tube Steels After Austenitizing—I. Chromium-Molybdenum Steels, *Arch. Eisenhuttenwes.*, 1980, **51**(8), p 355–360
13. C. Leumonie, J. Hennion, and L. Cadiou, Metallurgical Aspects of the Fabrication Aspects of Hydrocracking Equipment Made of 2.25% Cr-1% Mo, *Rev. Metall.*, 1974, **21**, p 683–697
14. T. Prnka, J. Purmensky, and A. Jakobova, The Influence of Thermo-mechanical Processing on the Microstructure and Mechanical Properties of 2¼ Cr-1%Mo Steel (15313), *Hutn. Listy*, 1971, **26**(1), p 51
15. T. Kunitake, T. Yukitoshi, K. Yoshikawa, and H. Ohtani, Continuous Cooling Transformations of Steels for High Temperature Service, *Sumitomo Kinzoku*, 1970, **22**(2), p 31–51
16. R. Ranjan and S.B. Singh, Bainite Transformation During Continuous Cooling: Analysis of Dilatation Data, *Metall. Mater. Trans. A*, 2018, **49A**(1), p 88–93
17. G.T. Eldis, A Critical Review of Data Sources for Isothermal Transformation and Continuous Cooling Transformation Diagrams, *Hardenability Concepts with Applications to Steel*, D.V. Doane and J.S. Kirkaldy, Ed., TMS-AIME, Warrendale, 1978, p 126–157
18. J. Trzaska and L.A. Dobrzanski, Modelling of CCT Diagrams for Engineering and Constructional Steels, *J. Mater. Process. Technol.*, 2007, **192**, p 504–510